Summary: A 2d3v numerical model of a DC sputter magnetron is presented. The model is fully self-consistent and kinetic. Based on the Particle-in-Cell/Monte Carlo Collisions technique it includes modules for the gas heating and the diffusion transport of the sputtered atoms. An external electric circuit is incorporated to achieve the calculation of the cathode voltage in a self-consistent manner, as well as the simulation of the constant current regime. The model is applied to a laboratory magnetron operated in argon.

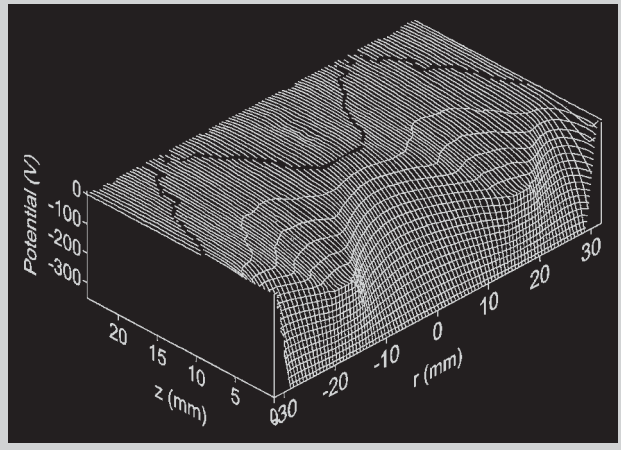

Calculated distribution of the electric potential, V, at $p =$ 10 mTorr. The white line corresponds to $V = 0$ V.

PIC – MCC Numerical Simulation of a DC Planar Magnetron

Ivan Kolev, Annemie Bogaerts*

Research group PLASMANT, Department of Chemistry, University of Antwerp, Universiteitsplein 1, 2610 Wilrijk, Belgium
E-mail: ivan.kolev@ua.ac.be

Received: September 26, 2005; Revised: December 13, 2005; Accepted: December 19, 2005; DOI: 10.1002/ppap.200500118

Keywords: magnetron; modeling; particles; plasma; sputtering

Introduction

Magnetrons are magnetically assisted glow discharges. This means that an external magnetic field is applied to the glow discharge to confine the plasma in the region immediately in front of the cathode. Due to this confinement, the discharge can operate at pressures as low as 1 mTorr with typical applied voltages from 250 to 500 V. The magnetic trap also ensures high plasma densities, exceeding 10^{17} m^{-3}. All that makes the magnetrons desired sources for sputtering and deposition of both metallic and non-metallic coatings. Sputter magnetrons in various configurations[1] have been in commercial use for several decades. Despite this fact, the physical processes happening during their operation are not yet fully understood. There are both theoretical and experimental reasons for that. The major theoretical obstruction comes from the experimentally known, but theoretically not yet satisfactorily explained anomalous diffusion across the magnetic lines. This means that applying the classic diffusion theory to a magnetron, working at typical magnetic fields of up to 0.1 T, leads to the wrong conclusion of almost no conductivity. The electrons should not be able to reach the anode, being trapped by the strong magnetic field. When it comes to experiments, the difficulties arise from the fact that the most intense plasma and correspondingly the key processes are located near the sheath, which in addition can be very thin (less than 1 mm). Thus, the information provided by probe measurements is somehow limited to a region of less interest. All above-mentioned reasons motivate the development of numerical models that can shed light over the processes in magnetrons.

Attempts for numerical models of magnetrons have been made for many years. Initially, different regions of the magnetron have been modeled. This includes, among others, a semi-analytical one-dimensional (1d) model of the cathode fall,[2] a 1d non-self-consistent fluid description,[3] and a pre-sheath model.[4] However, to provide a thorough insight, a model should be self-consistent, i.e., it has to include the calculation of the electric field based on the spatial distribution of the charged plasma species and the

applied external voltage. In other words, the model has to account for the coupling of the charged particle motion in the electric (or electromagnetic) field and the field itself, as it follows from the Poisson's equation. The dimensionality of the model should not be lower than required by the specifics of the magnetron. For cylindrical magnetrons, where the magnetic field can be thought as one-dimensional (1d) and constant in most of the discharge, a 1d self-consistent model yields good results.[5] In planar magnetrons, however, the magnetic field has a complex geometry and requires multi-dimensional treatment. In case of an axisymmetric magnetic field, it has been shown that the 2d cylindrical approach is correct.[6] It is worth to mention that the above discussion about the dimensionality refers to the coordinate space only. In the velocity space always the three components of the velocity are needed, in order to satisfy the energy conservation and to correctly describe the electron gyration around the magnetic field lines.

Further, the plasma in a discharge can, in principle, be treated as continuum (fluid) or kinetically. In magnetrons, however, when relatively strong magnetic fields are applied ($B > 150-200$ G) at low operating pressure ($p < 10$ mTorr), as it has been mentioned earlier, the classic transport coefficients become very low, which leads to unrealistic simulation results. This problem has been illustrated, in more detail, in ref.[7] In addition, the low pressures in the range of a few milliTorr make the fluid assumptions generally questionable. In attempt to overcome this problem a hybrid model has been proposed.[8] There, the ions are assumed to be a fluid, while the electrons are split into two groups: fast and slow. The slow group is again treated as a fluid. The fast electrons are followed individually by means of the Monte Carlo technique. The transport coefficients have been adopted from a separate study of the swarm parameters in crossed electric and magnetic fields by solving the Boltzmann's equation for argon.[9] This is a rather crude approximation because the electric and the magnetic fields in the planar magnetrons are not crossed, but conclude arbitrary angles. Another limitation originates from the criterion set to determine when a fast electron can be transferred into the slow group. In classical hybrid models of the discharges,[10] an electron is considered slow when its energy is less than some pre-set threshold and its location is outside the cathode fall. In the latter case, it is implicitly assumed that the discharge is with a net positive space charge, so that once outside the sheath, the electron cannot gain anymore energy. In magnetrons, operated at high-reduced magnetic fields, i.e., B/n, where B is the magnetic field and n is the feeding gas density, it has been shown that a negative space charge region (NSCR) can be formed;[5,7,11] thus, the electrons can gain energy in the entire discharge. Even without an NSCR, due to the gyration of the electrons, they can travel against the electric field for half a gyro-period and then in the second half they can again gain energy. An additional disadvantage of the fluid approach is that it cannot produce the energy probability functions for the electrons and ions. Because of all these arguments, a kinetic model should be used for a correct description of the magnetron discharges. The particle-in-cell-Monte Carlo collision technique (PIC-MCC)[12] satisfies this demand. Moreover, it has been shown[13] that in the limit of a small time step the PIC-MCC model converges to a solution of the Boltzmann's equation. So far, the PIC-MCC technique has been used to describe the behavior of the charged particles in a cylindrical DC magnetron (1d model),[5] in a planar DC magnetron (3d model with periodic boundary conditions),[6] and in an axisymmetric planar DC magnetron (2d model with an external circuit).[11]

In the present work, we propose a 2d self-consistent model based on the PIC-MCC technique where, in addition to the electrons and the feeding gas ions, also the sputtered atoms and their ions, metastable gas atoms, and the non-thermal gas atoms are included. To account for the possible collisional heating of the feeding gas a module, calculating the gas heating, is added. An external circuit, allowing the modeled discharge current to be limited and matched to the experimentally measured one, is incorporated as well.

Description of the Model

The presented model is two-dimensional in the coordinate space and three-dimensional in the velocity space. It is directly applicable to axisymmetric planar magnetrons and after moderate modifications can be used for magnetrons with arbitrary geometry. The flow chart of the entire simulation algorithm is shown in Figure 1. The first module is a PIC-MCC code for the electrons and the ions (Ar^+ and Cu^+). A general description of the PIC-MCC technique is given in.[12,14] All practical details and specific modifications used in this module are given in detail in a previous work.[11] Here only a brief description is given. The simulation starts with initial loading of electron and argon ion superparticles (SPs). They are chosen to be with homogeneous density corresponding to a real density equal to 10^{14} m^{-3}. Initial velocities are sampled from a Maxwellian distribution with temperatures of 1 eV for the electrons and 0.026 eV for the Ar^+ ions. The initial number of the SPs is equal to 90 000 for each type. During the simulation the number of SPs rises. To keep the simulation intensity under control an upper limit for their maximum number is set. When the limit is reached, the SPs are reduced twice on random basis. Correspondingly, their statistical weight is doubled. That is, after a reduction each SP represents twice as many real particles. The procedure of reduction conserves the total number and charge density, but cannot preserve the local current density. Thus, it is a potential source of numerical instabilities. Our experience shows that, if the reductions are applied less than five times

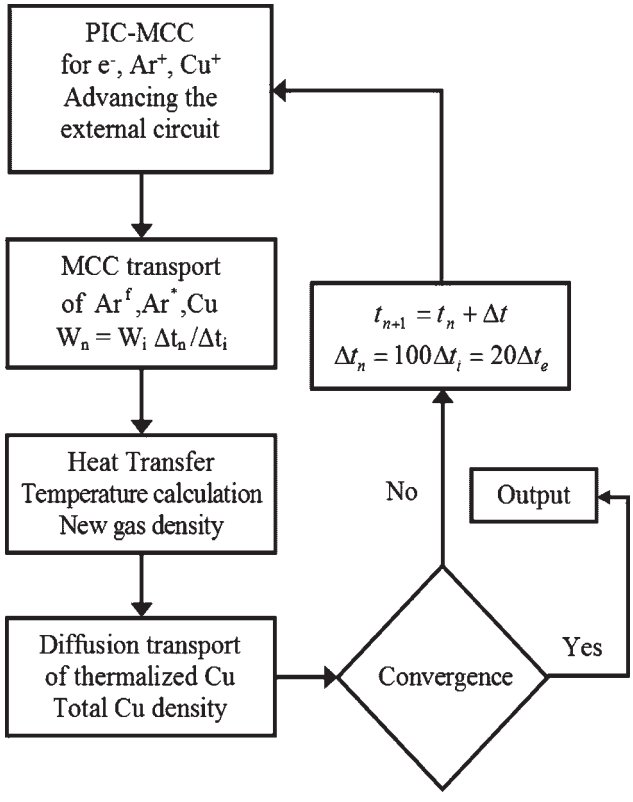

Figure 1. Flow chart of the simulation algorithm.

the system recovers. Otherwise, the weight of the SPs becomes too big and local fluctuations of the charge density appear, which evoke strong local variations of the electric field. This eventually makes the simulation unstable. The SPs are followed in each time step by Newton's laws. In the middle of each time step, the collision probability is calculated and compared to a uniformly distributed random number (*RN*) in the interval [0,1]. The sampling procedure is according to ref.[15] The following collisions are considered. For the electrons: collisions with argon atoms (elastic, excitation to metastable and radiative state, and single ionization), with copper atoms (elastic scattering and single ionization), with argon metastable atoms (transfer to a radiative state and single ionization), and with argon ions (recombination). For Ar^+ ions: with Ar (elastic, charge transfer, excitation to the metastable level, and single ionization) and with Cu^+ ions (asymmetric charge exchange). For Cu^+ ions: elastic scattering from Ar. In addition, Coulomb collisions are included. This is necessary having in mind that the conductivity in the magnetrons is caused by collisions, in contrast to the non-magnetized discharges. To accommodate multi-body collisions, such as Coulomb collisions, into a binary collision model, the algorithm proposed in ref.[16] has been implemented. For performing all collisions, except for those with the background gas, sorting is needed. That means it is necessary to know exactly which particles are at a given grid cell at a given time step. This sorting is performed according to the algorithm in ref.[17] For all binary collision processes, crosssection data from the literature have been used.[18–23] (see also in ref.[11]). At the end of each time step the potential, *V*, and the electric field are calculated, by solving the Poisson's equation

$$\frac{1}{r}\frac{\partial}{\partial r}r\frac{\partial V}{dr}+\frac{\partial}{\partial z}\frac{\partial V}{\partial z}=-\frac{q}{\varepsilon_0}(n_i-n_e)$$

where q is the elementary charge, ε_0 is the dielectric permittivity of free space, and n_i and n_e are the ion (Ar^+, Cu^+) and electron densities, respectively. The Poisson's equation is solved by means of the cyclic reduction method.[24] An essential feature of the model is the inclusion of the external circuit, consisting of a constant voltage source and a ballast resistor. It is shown in Figure 2. The role of the circuit is to provide a mechanism for limiting the simulated current. Without it the simulation can easily go to another region of the volt-ampere characteristic or even not converge at all. It is worth to say that the external circuit is not just a numerical trick, but an intrinsic part of the operation of any glow discharge and consequently a must for a self-consistent simulation. The coupling of the circuit to the discharge is by providing a boundary condition for the potential on the cathode.[11,25]

The next module deals with the transport and collisions of the neutrals. They include fast argon atoms (Ar^f), argon metastable atoms (Ar*), and sputtered copper atoms (Cu). The Ar^f are generated in elastic collisions of Ar^+, Ar^f, Ar*, Cu, and Cu^+ with Ar. An especially productive mechanism is the symmetric charge transfer between Ar^+ and Ar. The

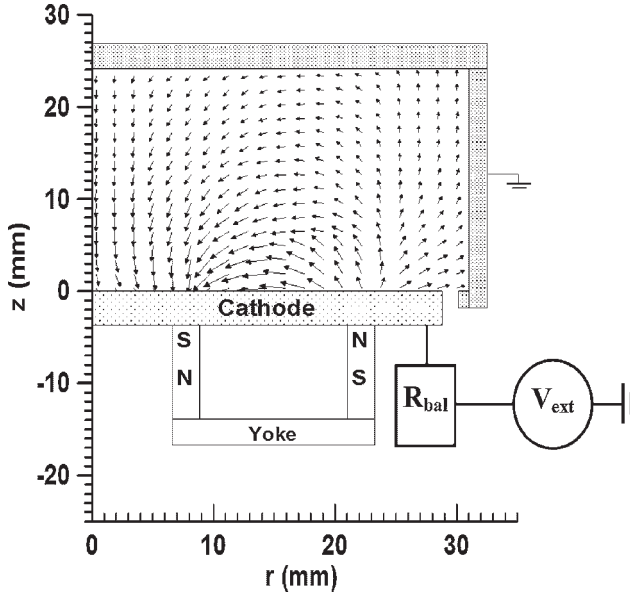

Figure 2. Scheme of the planar magnetron under consideration with the magnets and the magnetic field lines. The scheme is symmetrical towards the axis $r = 0$.

fast argon atoms are included in the model for two main reasons. First, they contribute to the sputtering. Second, when thermalizing by colliding with the slow argon atom population, they cause heating of the feeding gas, which can affect the discharge characteristics due to the dependence of the crosssections on gas density. The Ar^f are followed until thermalized, either by collisions or at the electrodes. The main reason for inclusion of the Ar* is to allow an additional mechanism for ionization of the Cu atoms, namely the process of Penning ionization. It has been shown that this can be a very important ionization path in the case of analytical glow discharges.[26] Ar* are created by electron-, Ar^+-, and Ar^f-impact collisions with the feeding gas. Their loss mechanism consists of electron-impact ionization and excitation to a radiative level, Penning ionization, deexcitation through collisions with Ar and Ar*, and deexcitation at the electrodes. The last is the most efficient mechanism at low gas pressure. Crosssection data have been taken from elsewhere.[27–29] The sputtered copper atoms are produced at the cathode by bombardment of Ar^+, Cu^+, and Ar^f. The probability for sputtering (the sputtering yield), Y, is calculated[30] as a function of the incident energy each time a bombardment happens

$$Y(\varepsilon_i) = 0.42\frac{\alpha Q K_s s_n(\varepsilon_i)}{U_s[1+0.35U_s s_e(\varepsilon_i)]}\left[1-(E_{th}/E)^{1/2}\right]^{2.8}$$

where ε_i is the energy of the incident particle, U_s is the sublimation energy of the cathode material, Eth is the threshold energy, and the other symbols are parameters related to the cathode material. This formula does not take into consideration the angular distribution of the incident flux. Y is compared to a RN. If $RN < Y$ a sputtered atom is released. For the energies of interest Y can be bigger than one. In that case one sputtered atom is always released. Next, the quantity, $(Y-1)$ is compared to a new RN. If bigger, a second sputtered atom is produced. The initial energy of the sputtered atoms, E_{sp}, is sampled from an approximation of the Thompson's distribution,[31] resulting in the relation$E_{sp} = U_s RN/(1-RN)$. This formula, however, has no upper limit. To keep the resulting energies physical a maximum acceptable energy, E_{max}, needs to be set. The maximum transfer energy in an elastic collision between the incident particle with a given energy and a target atom is used as such a maximum acceptable energy. E_{sp} is accepted if $E_{sp} < E_{max}$. Otherwise, a new sampling takes place. The angular distribution of the emitted Cu atoms is supposed to obey the cosine law. This means that the emission angle, Θ, measured from the normal to the target is sampled from $\Theta = \cos^{-1}(RN^{1/2})$. The azimuthal angle, φ, is taken to be a random fraction of 2π, that is $\varphi = 2\pi RN$. The RNs in the formulae for the two angles are independent. In the case of elastic collisions of Cu with Ar, anisotropic scattering is considered. The scattering angle is determined as a function of the relative energy.[32] At the electrodes Cu atoms are assumed to have a sticking coefficient equal to one. Thus, in the calculation of the sputter flux, back-deposition is taken into consideration.

The different processes in the magnetron have different characteristic times. This fact leads to large disparity of the necessary time steps for the electrons, ions, and the neutrals. The shortest time step is needed for the electrons to resolve the electron plasma frequency and the electron gyrofrequency. On the other hand, such small time step, in the picosecond order, is unusable in the neutral's collision. Moreover, to allow a steady state in terms of the thermal conductivity of the feeding gas, the simulation needs to be carried until 10^{-2} s. With the electron time step, this is a formidable task for the contemporary computers. To cope with this problem the simulation is carried with different time steps: $\Delta t_e \ll \Delta t_i \ll \Delta t_n$ (e-electron, i-ion, and n-neutral). At the same time the weights are also different in order to compensate for the differences in the time steps and to assure that the production and loss rates of the real plasma particles are correctly represented. This is achieved by choosing

$$W_n = W_i\frac{\Delta t_n}{\Delta t_i}$$

where W_n is the weight of the neutrals and W_i is the weight of the charged particles. Note that the electrons and the ions have the same weight, but different time steps. In this case electron subcycling is used, i.e., inside one ion time step the electrons are advanced (subcycled) n times. In the present model $n = 20$. Thus, the overall cycle consists of one ion time step. At the end of it the power density, P, transferred to and from the feeding gas is accumulated

$$P = \frac{m_g W_n}{V\Delta t_n}\left[\sum_l \frac{v_l'^2 - v_l^2}{2} - \sum_l{}' \frac{v_l^2}{2} + \sum_l{}'' \frac{v_l'^2}{2}\right]$$

where v_l' is the post- and v_l is the pre-collision velocity of the lth gas atom, m_g is the gas mass, and V is the volume of the computational grid cell. The first sum is the contribution from all collisions between the feeding gas atoms from one side and the ions, fast atoms, metastable atoms, and sputtered atoms from the other side. Only collisions in which the post-collision energy of the gas atom is less than some threshold are counted. This threshold is chosen to be $E_{th} = 9 \times (3/2)k_b T_g$.[33] The other collisions result in creating of fast gas atoms, which are incorporated by the second sum. The third sum is the contribution of the thermalized fast gas atoms. This calculated power density is used as a source term in the thermoconductivity equation

$$\frac{\partial^2 T_g}{\partial z^2} + \frac{1}{r}\frac{\partial}{\partial}\left(r\frac{\partial T_g}{\partial r}\right) = -\frac{P}{k}$$

which is solved once per one hundred ion time steps to calculate the gas temperature, T_g. In the above equation k is

the thermal conductivity of the gas. In the case of Ar it is taken to be[34] $k = 0.018\ \mathrm{W \cdot m^{-1} \cdot K^{-1}}$.

The simulation is carried out until a steady state is achieved. This is judged by tracing in time the calculated cathode voltage, the total number of SPs for each type of plasma species, the average ionization rate, and the maximum densities for each type of SPs. When the average values of these quantities do not change during 5 000 time steps with more than 1%, the simulation is stopped. Usually it takes from two to five millions time steps depending on the pressure, the longest times corresponding to the lowest pressures.

Results and Discussion

The model is applied to the magnetron presented in Figure 2. It is a planar DC magnetron Von Ardenne PPS50 with an axisymmetric magnetic field, operated in argon with a copper cathode. The magnetic field is also shown in Figure 2. It has a maximum value of about 0.12 T in the region immediately before the cathode at a radial position, $r = 18$ mm. The magnetic field has been measured[35] and is an input in the model. It is considered to be strong enough, in order not to be influenced by the internal magnetic field created by the movement of the charges in the discharge.

The external circuit parameters are: $V_{ext} = 750$ V, $R_{bal} = 1\,200–2\,000\ \Omega$. The initial gas temperature is assumed to be 300 K. All simulations are performed keeping the calculated current approximately equal to 300 mA.

The convergence of the numerical procedure is illustrated in Figure 3, where the calculated external and plasma cathode currents are shown. The latter is defined by the charged plasma flux at the cathode. At steady state they should coincide and be quasi-constant. As it can be seen, the steady state happens approximately at 12 μs after the beginning of the simulation. Next, typical results of the model, such as the calculated discharge potential distribution, plasma densities, and temperature profile, are presented for the case of $p = 10$ mTorr. Finally, the pressure dependence of the sputter flux and temperature is given for the range, $p = 1–100$ mTorr.

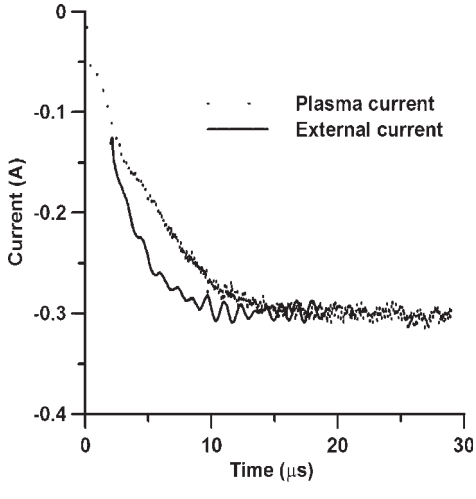

Figure 3. Simulated external and plasma currents as a function of time.

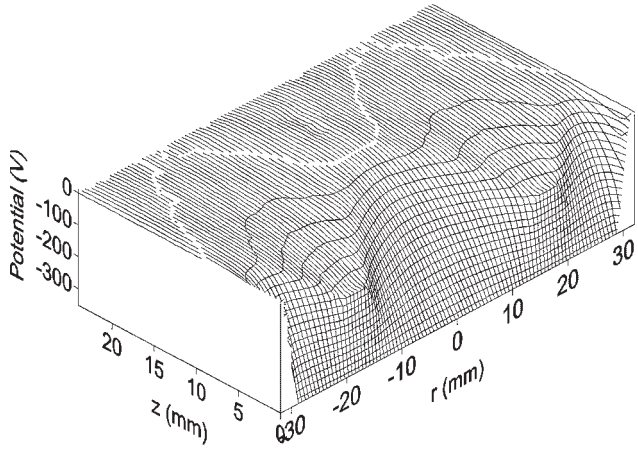

Figure 4. Calculated distribution of the electric potential, V, at $p = 10$ mTorr. The white line corresponds to $V = 0$ V.

In Figure 4, the calculated distribution of the potential, V, is shown. Two zones can be distinguished. The first zone is located between the poles of the magnet. It is characterized by strong entrapment of the electrons, creating a negative space charge. It is in this zone where most of the plasma is concentrated, as it can be seen in Figure 5–8. The sheath thickness, d, has a strong radial dependence. It has a minimum, $d_{min} = 1.2$ mm, at $r = 18$ mm, where the radial component of the magnetic field is strongest. The second zone is above the center of the cathode, where the space charge is positive. There the plasma is very weakly magnetized and d has a maximum, $d_{max} = 14$ mm. The electric field reaches very strong values in the sheath up to $600\ \mathrm{kV \cdot m^{-1}}$.

The electron density distribution (Figure 5) is very well localized in the region between the magnet poles and has a

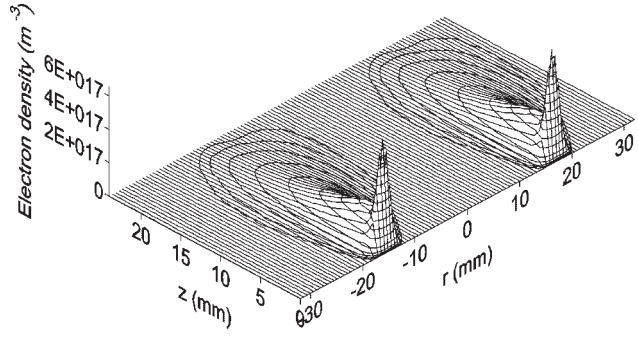

Figure 5. Calculated density distribution of the electrons at $p = 10$ mTorr.

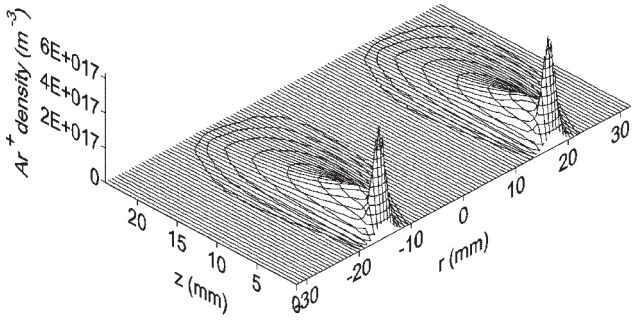

Figure 6. Calculated density distribution of the Ar^+ ions at $p = 10$ mTorr.

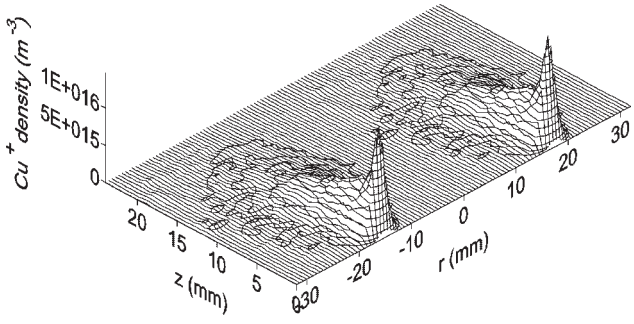

Figure 7. Calculated density distribution of the Cu^+ ions at $p = 10$ mTorr.

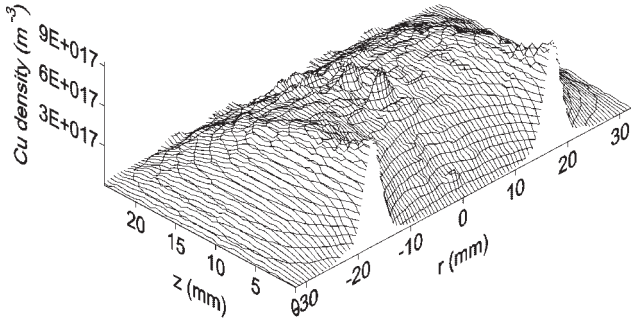

Figure 8. Calculated density distribution of the Cu atoms at $p = 10$ mTorr.

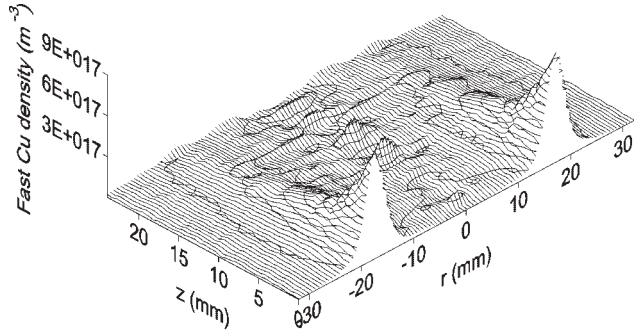

Figure 9. Calculated density distribution of the fast Cu atoms at $p = 10$ mTorr.

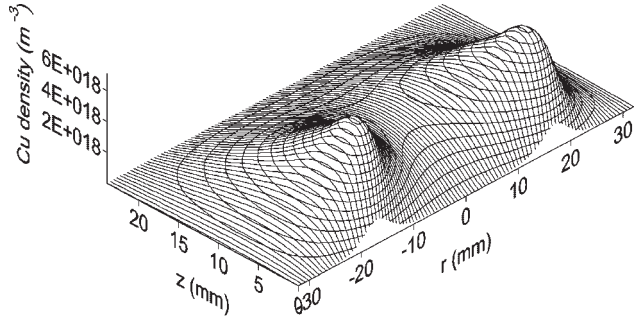

Figure 10. Calculated density distribution of the Cu atoms at $p = 100$ mTorr.

maximum value of $n_e = 6 \times 10^{17}$ m^{-3}. Except in the sheath, the Ar^+ density (Figure 6) follows the electron density. Although practically not magnetized under the current operating conditions, the Ar^+ ions are electrostatically bound to the electrons.

The sputtered atoms are partially ionized. The degree of ionization is about 2%. The calculated density profile of the Cu^+ ions is shown in Figure 7. It has a maximum of approximately 1.5×10^{16} m^{-3}. Thus, the main positive charge is due to the Ar^+ ions. Comparing Figure 6 and 7 it can be seen that the Cu^+ density is less confined than the Ar^+ density. This can be explained with the relative contribution of the Penning ionization. Ar* atoms (not shown here) are relatively homogeneously distributed and correspondingly the creation of Cu^+ ions is less spatially concentrated.

The sputtered atom density distribution (Figure 8) has a maximum of approximately 9×10^{17} m^{-3}. Due to the low pressure and the small discharge cell, there is a non-negligible fraction of Cu atoms with energies of a few eV, which reach the opposite wall, where normally a substrate is mounted. This is illustrated in Figure 9, where the calculated density profile of the fast Cu atoms is shown. As it can be seen this density is not equal to zero near the opposite to the cathode wall. According to our calculations at increased pressures, the majority of the fast Cu atoms thermalize before reaching the anode. This can be seen in Figure 10 and 11, where the same quantities as in Figure 8 and 9 are shown, but for $p = 100$ mTorr. In this case the calculated Cu atom density above the racetrack has a typical diffusion-dominated profile.

The calculated gas temperature is shown in Figure 12. It has a maximum of 312 K. The results of the model show that the effect of gas heating can be neglected for pressures of up to 10 mTorr. At higher pressures, however, the effect is significant and should be considered, as it follows from Figure 13, where the maximum temperature of the discharge as a function of the pressure is plotted.

In Figure 14 the relative contribution of the bombarding particles to the sputtered flux is shown. For the given

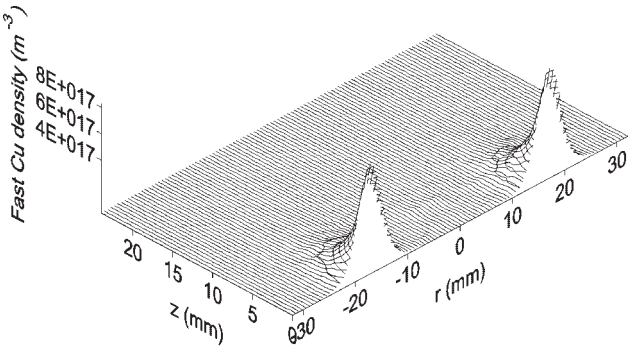

Figure 11. Calculated density distribution of the fast Cu atoms at $p = 100$ mTorr.

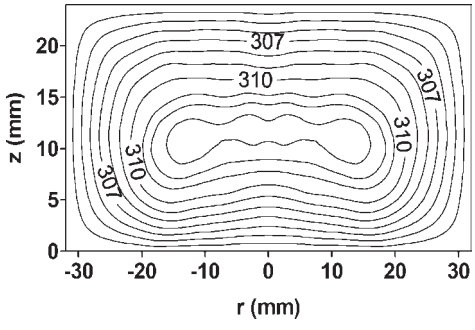

Figure 12. Calculated gas temperature distribution (K) at $p =$ 10 mTorr.

conditions, the Ar^+ ions account for 83% of the sputtering. The role of Cu^+ ions is marginal. The effect of pressure upon the total sputter flux (back-deposition included) is given in Figure 15. Initially the maximum of the sputter flux increases with pressure, which can be expected, because the ionization rate of argon gas increases with pressure as well. Above 10 mTorr, however, the maximum of the sputter flux

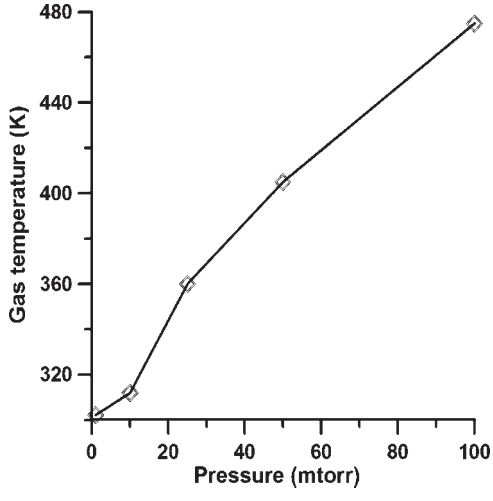

Figure 13. Calculated gas temperature as a function of the gas pressure. The open diamonds represent the simulated values.

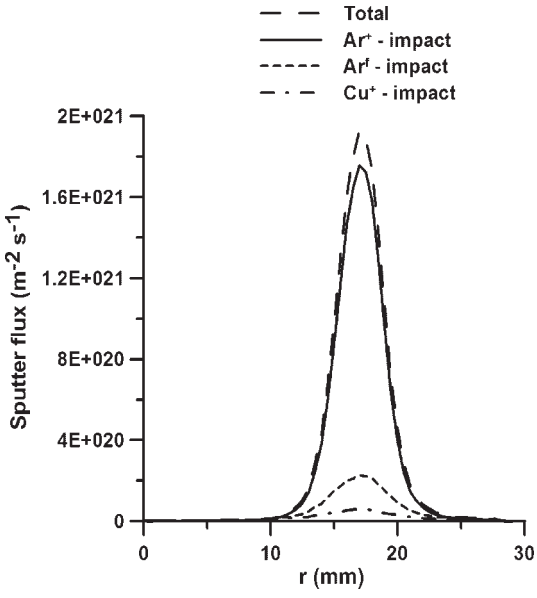

Figure 14. Relative contribution of the different plasma species to the calculated sputter flux $p = 10$ mTorr.

begins to decrease with the pressure. The width of the sputter flux profile, measured at 0.7 of the maximum height, increases monotonically with the pressure. Two factors may contribute to that. First, the influence of the symmetric charge transfer collisions in the sheath and the pre-sheath increases with the pressure, thus leading to lower ion bombarding energies and a lower sputtering yield. The radial broadening of the profile can also be attributed to the higher number of Ar^+-Ar collisions, which deteriorate the directionality of the ions striking the cathode.

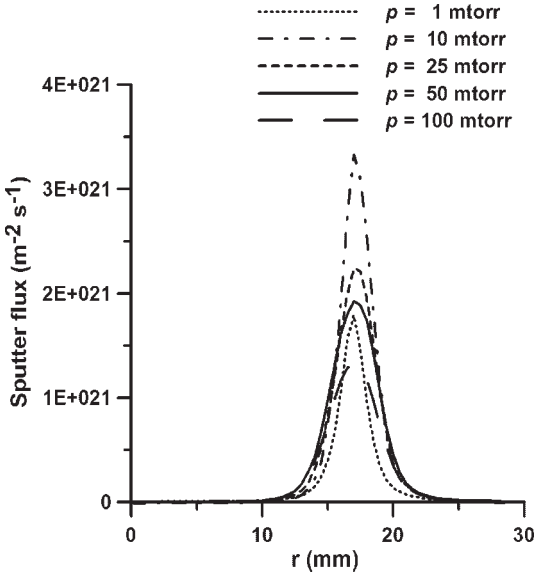

Figure 15. Calculated sputter flux as a function of the gas pressure.

Second, the back-deposition of the sputtered atoms manifests stronger, due to the higher rate of Cu-Ar collisions.

Conclusion

A detailed and realistic numerical model for simulations of magnetron sputtering systems has been presented. The model is able to produce the most important discharge characteristics without any limiting assumptions. The results show that for the given operational conditions a region with a negative space charge is formed, due to the extremely limited electron mobility. The plasma is very well confined in the region between magnetic poles, and the main source for sputtering are the Ar^+ ions. The effect of gas heating is important at higher pressures and can be neglected in the range of 1–10 mTorr.

The model is not limited to Ar gas only or to some specific operating conditions. It needs modification only for the case of non-axisymmetric magnetic field and can relatively easily be adapted for rf or pulsed discharges.

[1] J. A. Thornton, in: "*Thin Film Processes*", J. L. Vossen, W. Kern, Eds., Academic, New York 1978, p. 76.
[2] W. Bradley, G. Lister, *Plasma Sources Sci. Technol.* **1997**, *6*, 524.
[3] L. Pekker, *Plasma Sources Sci. Technol.* **1995**, *4*, 31.
[4] J. W. Bradley, *Plasma Sources Sci. Technol.* **1998**, *7*, 572.
[5] T. A. van der Straaten, N. F. Cramer, I. S. Falconer, B. W. James, *J. Phys. D: Appl. Phys.* **1998**, *31*, 177 and 191.
[6] S. Kondo, K. Nanbu, *J. Phys. D: Appl. Phys.* **1999**, *32*, 1142.
[7] I. Kolev, A. Bogaerts, *Contrib. Plasma Phys.* **2004**, *7–8*, 582.
[8] E. Shidoji, H. Ohtake, N. Nakano, T. Makabe, *Jpn. J. Appl. Phys., Part 1* **1999**, *38*, 2131.
[9] K. Ness, T. Makabe, *Phys. Rev. E* **2000**, *62*, 4083.
[10] A. Bogaerts, R. Gijbels, W. J. Goedheer, *J. Appl. Phys.* **1995**, *78*, 2233.
[11] I. Kolev, A. Bogaerts, R. Gijbels, *Phys. Rev. E* **2005**, *72*, 056402.
[12] C. K. Birdsall, *IEEE Trans. Plasma Sci.* **1991**, *19*, 66.
[13] H. Babovsky, R. Ilner, *SIAM J. Num. Anal.* **1989**, *26*, 45.
[14] C. K. Birdsall, A. B. Langdon, "*Plasma Physics via Computer Simulations*", IOP, Bristol 1991.
[15] K. Nanbu, *Jpn. J. Appl. Phys., Part 1* **1994**, *33*, 4752.
[16] K. Nanbu, S. Yonemura, *J. Comput. Phys.* **1998**, *145*, 639.
[17] K. Bowers, *J. Comput. Phys.* **2001**, *173*, 393.
[18] N. J. Mason, W. R. Newell, *J. Phys. B* **1987**, *20*, 1357.
[19] H. A. Hyman, *Phys. Rev. A* **1979**, *20*, 855.
[20] H. A. Hyman, *Phys. Rev. A* **1978**, *18*, 441.
[21] D. P. Lymberopoulos, D. J. Economou, *J. Appl. Phys.* **1993**, *73*, 3668.
[22] M. A. Biondi, *Phys. Rev.* **1963**, *129*, 1181.
[23] A. Bogaerts, R. Gijbels, *J. Appl. Phys.* **1996**, *79*, 1279.
[24] P. N. Swartztrauber, *SIAM J. Numer. Anal.* **1974**, *11*, 1136.
[25] V. Vahedi, G. DiPeso, *J. Comput. Phys.* **1996**, *131*, 149.
[26] A. Bogaerts, R. Gijbels, *Phys. Rev. A* **1995**, *52*, 3743.
[27] C. M. Ferreira, J. Loureiro, A. Ricard, *J. Appl. Phys.* **1985**, *57*, 82.
[28] L. A. Riseberg, W. F. Parks, L. D. Schearer, *Phys. Rev. A* **1973**, *8*, 1962.
[29] C. M. Ferreira, A. Ricard, *J. Appl. Phys.* **1983**, *54*, 2261.
[30] N. Matsunami, Y. Yamamura, Y. Itikawa, N. Itoh, Y. Kazumata, S. Miyagawa, K. Morita, R. Shimizu, H. Tawara, *Atom. Data Nucl. Data Tables* **1984**, *31*, 1.
[31] M. W. Thompson, *Philos. Mag.* **1968**, *18*, 377.
[32] J. Sielanko, *Rad. Eff. Lett.* **1984**, *86*, 185.
[33] V. Serikov, K. Nanbu, *J. Appl. Phys.* **1997**, *82*, 5948.
[34] R. L. Powell, G. E. Childs, "*American Institute of Physics Handbook*", D. E. Gray, Ed., McGraw-Hill, New York 1972.
[35] G. Buyle, private communication.

